



## The transport along membrane nanotubes driven by the spontaneous curvature of membrane components

Doron Kabaso<sup>a,b,1</sup>, Nataliya Bobrovskaya<sup>c,1</sup>, Wojciech Gózdź<sup>c</sup>, Ekaterina Gongadze<sup>a</sup>, Veronika Kralj-Iglič<sup>d,e</sup>, Robert Zorec<sup>b,f</sup>, Aleš Iglič<sup>a,e,\*</sup>

<sup>a</sup> Laboratory of Biophysics, Faculty of Electrical Engineering, University of Ljubljana, Tržaška cesta 25, SI-1000 Ljubljana, Slovenia

<sup>b</sup> Laboratory of Neuroendocrinology-Molecular Cell Physiology, Faculty of Medicine, University of Ljubljana, Ljubljana, Slovenia

<sup>c</sup> Institute of Physical Chemistry, Polish Academy of Sciences, Warsaw, Poland

<sup>d</sup> Faculty of Health Studies, University of Ljubljana, Zdravstvena 5, SI-1000 Ljubljana, Slovenia

<sup>e</sup> Laboratory of Clinical Biophysics, Department of Orthopaedics, Faculty of Medicine, University of Ljubljana, Zaloška 9, SI-1000 Ljubljana, Slovenia

<sup>f</sup> Celica, Biomedical Center, Technology Park, 1000 Ljubljana, Slovenia

### ARTICLE INFO

#### Article history:

Received 4 August 2011

Received in revised form 20 February 2012

Accepted 28 February 2012

Available online 14 March 2012

#### Keywords:

Computational model

Membrane and cell biomechanics

Intercellular nanotubes

Transport mechanism

Nanotube dilations (gondolas)

### ABSTRACT

Intercellular membrane nanotubes (ICNs) serve as a very specific transport system between neighboring cells. The underlying mechanisms responsible for the transport of membrane components and vesicular dilations along the ICNs are not clearly understood. The present study investigated the spatial distribution of anisotropic membrane components of tubular shapes and isotropic membrane components of spherical shapes. Experimental results revealed the preferential distribution of CTB (cholera toxin B)–GM1 complexes mainly on the spherical cell membrane, and cholesterol–sphingomyelin at the membrane leading edge and ICNs. In agreement with previous studies, we here propose that the spatial distribution of CTB–GM1 complexes and cholesterol–sphingomyelin rafts were due to their isotropic and anisotropic shapes, respectively. To elucidate the relationship between a membrane component shape and its spatial distribution, a two-component computational model was constructed. The minimization of the membrane bending (free) energy revealed the enrichment of the anisotropic component along the ICN and the isotropic component in the parent cell membrane, which was due to the curvature mismatch between the ICN curvature and the spontaneous curvature of the isotropic component. The equations of motion, derived from the differentiation of the membrane free energy, revealed a curvature-dependent flux of the isotropic component and a curvature-dependent force exerted on a vesicular dilation along the ICN. Finally, the effects of possible changes in the orientational ordering of the anisotropic component attendant to the transport of the vesicular dilation were discussed with connection to the propagation of electrical and chemical signals.

© 2012 Elsevier B.V. All rights reserved.

### 1. Introduction

Experimental studies have shown that inter-cellular membrane nanotubes (ICNs) can be found in a variety of cell types [33,38,39,28,23,5,40] representing a natural communicative system between neighboring cells. Previous theoretical studies suggested that the membrane composition might have a role in the stability of the ICN [8] and the membrane component transport along the ICN. To date, the membrane composition of the ICN remains largely unknown [3,8,16,41]. By using raft markers, we revealed the absence of CTB–GM1 complexes and the presence of cholesterol–sphingomyelin rafts in the ICN of malignant (T24) cancer cells of urothelial origin (Fig. 1). The observed spatial segregation

could be explained by assuming that CTB–GM1 complexes and cholesterol–sphingomyelin rafts have isotropic and anisotropic shapes, respectively. In the first part of the present two-component theoretical model, the minimization of the free (bending) energy with respect to the shape of the vesicle and the distribution of the components on the vesicle surface revealed the aggregation of the isotropic component in the spherical cell compartment and the anisotropic component in the ICN. In the second part, the curvature-dependent flux of the isotropic component and the force exerted on a newly formed vesicular dilation were derived from the system free energy.

The communication through ICNs allow the passage of signaling molecules, cytoskeletal components, and organelles [33,15]. This communication is also important to cell growth, cell shaping, and cell mobility, which is also observed in the osteointegration of orthopedic implants [20,29–31]. Previous studies have shown that molecular motors moving on the inner cytoskeleton may drive the incorporation and transport of vesicular dilations and incorporated organelles along the ICN [33,38,39,12,2]. Yet, the transport of vesicular dilations

\* Corresponding author at: Laboratory of Biophysics, Faculty of Electrical Engineering, University of Ljubljana, Tržaška cesta 25, SI-1000 Ljubljana, Slovenia. Tel.: +386 1 4768 825; fax: +386 1 4768 850.

E-mail address: [doron.kabaso@fe.uni-lj.si](mailto:doron.kabaso@fe.uni-lj.si) (Doron Kabaso).

<sup>1</sup> The first two authors equally share the first authorship.

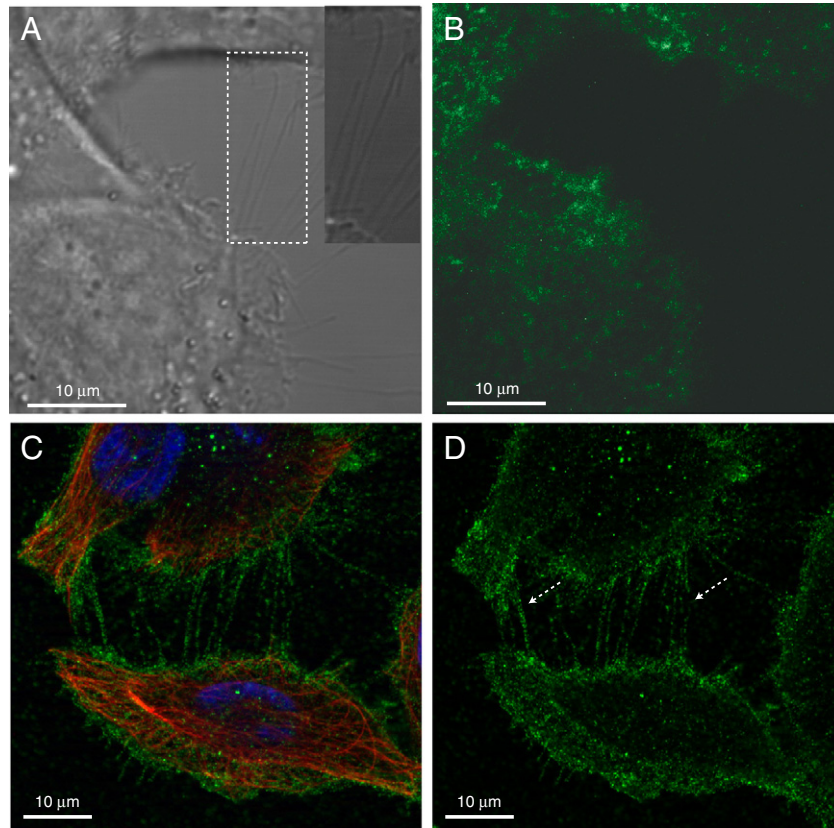


**Fig. 1.** Confocal images demonstrating the aggregation of CTB–GM1 complexes on the spherical cell membrane and cholesterol–sphingomyelin rafts on inter-cellular membrane nanotubes (ICNs). A phase contrast image of CTB treated T24 cells (A). Note the presence of ICNs (see inset) between neighboring cells. Fluorescence image reveals the presence of CTB–GM1 complexes (in green) on the plasma membrane and not on the ICNs (B). The aggregation of cholesterol–sphingomyelin rafts (in green) on the cell membrane edges and ICNs (C). Note the integrity of microtubules (in red), nucleus (in blue), and cholesterol–sphingomyelin rafts (in green). Cholesterol–sphingomyelin rafts marked by Ostreolysin (Oly) are distributed on ICNs (see arrows; D).

was also possible in artificial systems such as giant unilamellar vesicles (GUVs) that exclude the inner cytoskeleton and molecular motors [25,27,39]. Previously, it was suggested that the dilation transport could also be mediated by a membrane tension gradient [19,4]. It has been demonstrated that a mechanical pressure on a vesicle connected by an ICN may lead to a flux of lipids and cytoplasm towards the tensed vesicle [4]. Herein, we propose that a perturbation in the membrane tension could originate from changes in the spontaneous curvature (i.e. the intrinsic curvature and density) of the membrane components residing along the tubular ICN.

A membrane component was previously defined as anisotropic or isotropic, when its intrinsic curvatures (describing intrinsic shape) [7,16,18,39] along the two principal directions were different or of similar magnitudes, respectively (Fig. 2). A membrane component

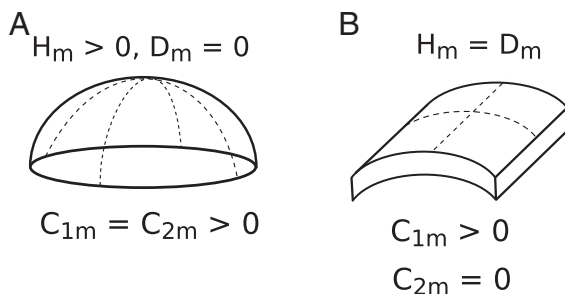


**Fig. 2.** A schematic figure of a membrane domain having isotropic ( $D_m = 0$ ) spontaneous curvature of a spherical shape (A) and anisotropic ( $D_m > 0$ ) spontaneous curvature of a cylindrical shape (B). Note that  $C_{1m}$  and  $C_{2m}$  are the intrinsic (spontaneous) membrane curvatures.

could represent a single molecule or a membrane nanodomain, which bends the membrane or stabilizes the cell membranes [32,21]. Recent theoretical studies have demonstrated lateral segregation or even complete phase separation of anisotropic components of cylindrical spontaneous curvature in the ICN and isotropic components of spherical spontaneous curvature in the parent membrane [17,37,24]. The phase separation was driven by the difference between the intrinsic (spontaneous) curvature of the anisotropic membrane component and the tube membrane curvature. Due to the nearly flat (i.e. small curvature) parent cell membrane, the equilibrium concentration of the isotropic component was greater in the parent cell membrane than in the tube membrane. It was also revealed that the formation of a vesicular dilation could be facilitated, when the spontaneous curvature of the isotropic component matched the vesicle curvature. In the discussion, we explain how the restoring membrane force that works to flatten the newly formed vesicular dilation can be exploited for the vesicle transport along the ICN.

## 2. The spatial distribution of membrane components

Urothelial cell line T24 was cultured in a 1:1 mixture of advanced Dulbecco's modified Eagle's medium (Gibco, Invitrogen, Carlsbad, CA, USA) and Ham's F-12 (Sigma-Aldrich Corp., St. Luis, MO, USA), supplemented with 10% FBS (Gibco, Invitrogen, Carlsbad, CA, USA), 5  $\mu\text{g}/\text{ml}$  insulin, 5  $\mu\text{g}/\text{ml}$  transferrin, 100  $\text{mg}/\text{ml}$  hydrocortisone and 5  $\text{ng}/\text{ml}$  selenite (all Gibco, Invitrogen, Carlsbad, CA, USA), 1800 U/ml cristacyclin (Pliva, Zagreb, Croatia) and 0.222  $\text{mg}/\text{ml}$  streptomycin sulfate (Fatol Arzneimittel GmbH, Schiffweiler, Germany). Cells were incubated at 37  $^\circ\text{C}$  in a humidified incubator in an atmosphere of 5%  $\text{CO}_2$ . A day prior to experiment, cells were seeded onto sterile glass coverslips

(Brand GmbH, Wertheim, Germany) at approximately 70–80% confluence and incubated overnight at 37 °C.

Ostreolysin (Oly) was isolated from fresh fruiting bodies of *P. ostreatus* as described. The purity of Oly was checked by polyacrylamide gel electrophoresis. The protein concentration was determined spectrophotometrically using the BCA Protein Assay Reagent (Pierce, USA). After isolation, the protein was desalted and kept frozen (–20 °C) in aliquots in 140 mM NaCl, 1 mM EDTA, 20 mM Tris–HCl buffer, pH 8.0. Rabbit anti-Oly primary antibodies were prepared as described [1]. T24 cells grown on coverslips were incubated with 2.5 µg/ml of Oly for 30 min at 37 °C. After fixation in 4% PA, washing with PBS and blocking with 2% BSA with 0.2% sodium azide, we added primary Oly anti-rabbit antibodies (1:2500), and then Alexa Fluor 555-conjugated secondary antibodies (1:1000) (Molecular Probes, Oregon, USA). Coverslips were washed and mounted in Vectashield with DAPI (Vector Laboratories, Burlingame, CA).

A stock solution of fluorescent cholera toxin-B conjugate (component A of Vybrant Alexa Fluor 488 Lipid Raft Labeling Kit (Molecular Probes, Invitrogen, USA)) was diluted to a final concentration of 4 µg/ml in PBS and added to the washed cells on glass coverslip. Cells were incubated in CTB solution for 20 min at room temperature or at 37 °C in humidified chamber, then washed with PBS and fixed in 2% formaldehyde in PBS for 30 min. The integrity of microtubule filaments was evaluated by labeling with anti-tubulin and the nucleus was labeled with DAPI.

T24 cells were cultured on glass bottom dishes (MatTek Corporation, Ashland, MA, USA). Images were obtained on a LSM 510 (Carl Zeiss) confocal microscope using transmission light (oil objective 63). To label GM1s or cholesterol–sphingomyelin rafts, we added CTB or Oly, respectively. Fig. 1 shows the preferential distribution of CTB–GM1 complexes on the spherical cell membrane (Fig. 1B) and the preferential distribution of cholesterol–sphingomyelin rafts on the leading edge of the membrane and ICNs (Fig. 1D). Previously, it was suggested that the CTB–GM1 complex has a positive and isotropic spontaneous curvature, while the spontaneous curvature of the cholesterol–sphingomyelin raft could be anisotropic [35,23].

### 3. The phase separation of isotropic and anisotropic components

In this section, we investigated a model of two-component membrane with anisotropic component (B) and isotropic component (A), which were characterized by different intrinsic curvatures (Fig. 2). The aim was to elucidate the influence of anisotropic membrane domains on the shape transformations of the closed neighboring cells connected by an ICN. The coupling between changes in the membrane shape and the lateral distribution of membrane components could lead to lateral segregation of the membrane components [17,37,36]. The ICN might coincide with nearly complete lateral segregation of membrane components, where the anisotropic components (domains) were accumulated in the ICN and the isotropic components in the connected neighboring parent cells. The membrane free energy, taking into account the anisotropy of membrane components, was considered within continuum approach in the generalized Helfrich form [6,26,7,16]:

$$F = \int \left( \kappa \left( (H - H_m(\phi))^2 + (D - D_m(\phi))^2 \right) + \frac{kT}{a_0} (\phi \ln(\phi) + (1 - \phi) \ln(1 - \phi)) \right) dA, \quad (1)$$

where  $\kappa$  is the membrane bending modulus,  $H = (C_1 + C_2)/2$  is the mean membrane curvature,  $D = |C_1 - C_2|/2$  is the curvature membrane deviator,  $C_1$  and  $C_2$  are the principal curvatures,  $H_m(\phi) = (C_{1m} + C_{2m})/2$  is the intrinsic (spontaneous) membrane curvature and  $D_m(\phi) = |C_{1m} - C_{2m}|/2$  is the intrinsic (spontaneous) curvature membrane deviator,  $C_{1m}$  and  $C_{2m}$  are the two intrinsic principal curvatures,  $\phi$  is the local relative concentration of the A component and  $dA$  is the infinitesimal membrane

area element. The last term in Eq. (1) is the entropy of mixing (see also Supplementary material), where  $a_0$  is the area per single membrane component of type A,  $\kappa$  is the Boltzmann constant, and  $T$  is the temperature. The integral is taken over the surface of the vesicle. The difference between the membrane curvature and the membrane intrinsic (spontaneous) curvature determined the energy cost for bending the membrane away from its favorable curvature. It was assumed that the total relative densities of the A and B components equalled unity. The intramolecular interactions between the components were neglected in Eq. (1).

In our model, the local relative density of the A component ( $\phi$ ) affected on the intrinsic mean and deviatoric membrane curvatures of the membrane, as follows:

$$\begin{aligned} H_m(\phi) &= (H_m^A - H_m^B)\phi + H_m^B \\ D_m(\phi) &= (D_m^A - D_m^B)\phi + D_m^B, \end{aligned} \quad (2)$$

where  $H_m^A$  and  $H_m^B$  are the spontaneous (intrinsic) mean curvatures and  $D_m^A$  and  $D_m^B$  are spontaneous (intrinsic) curvature deviators of components A and B, respectively.

We minimized the functional Eq. (1) for axisymmetric vesicles at constraint of constant reduced volume  $v$  and constraint of conserved total number of A components, given as  $\phi_{tot} = \int \frac{\phi dA}{A}$ . The reduced volume was the ratio of the volume of the vesicle to the volume of the sphere with the same surface area as a given vesicle. The vesicle shape was parametrized with the angle that forms a tangent to the shape profile with the rotational axis as a function of the arclength  $s$  [9–11]. The relative concentration of A component ( $\phi$ ) is a function of arclength  $s$  given by  $\phi(s) = 1 - (\frac{1}{2} \Delta\phi [\tan h(\xi(s-s_0)) - \tan h(\xi(s-s_0 - \Delta s_0))] + \phi_c)$ , where  $s_0$  is the position of the boundary between the region rich in component A and the region rich in component B,  $\xi$  is the slope of the concentration profile at  $s_0$ ,  $\Delta s_0$  is distance between inflection points of two hyperbolic tangents and  $\Delta\phi = \phi_t - \phi_c$ , where  $\phi_t$  and  $\phi_c$  are the maximal concentration of component A in the tubular region and minimal concentration of component A outside the tubular region. Parameters  $s_0$ ,  $\Delta s_0$ ,  $\phi_t$ , and  $\phi_c$  are determined during the minimization process.

Fig. 3 shows the aggregation of the isotropic component in the parent spherical membrane and the anisotropic component in the ICN. By excluding the effects of entropy, the ICN membrane favored the anisotropic (B) component, while the isotropic component was energetically more favorable in the neighboring parent cells (Fig. 3A). The deviatoric energy of the anisotropic component attained its minimum upon the

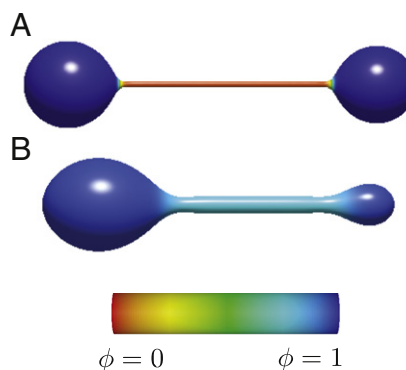


**Fig. 3.** The calculated equilibrium closed membrane shapes obtained in a system of isotropic components and anisotropic components are drawn without (A) and (B) the inclusion of the entropy term. In the color map, the hot colors (e.g. red) denote more of the B (anisotropic) component, and the cold colors (e.g. blue) denote more of the A (isotropic) component. Note that the segregation of components is reduced following the inclusion of the entropy term. The calculations are performed for  $\phi_{tot} = 0.92$  and  $\bar{H}_m^B = 11$ ,  $\bar{H}_m^A = 3$ , and for the reduced volume  $v = 0.63$ . The spontaneous curvature deviators were  $\bar{D}_m^B = 11$  and  $\bar{D}_m^A = 0$ . The values of intrinsic curvatures (e.g.  $C_{1m}$  and  $C_{2m}$ ) are presented in dimensionless units defined with analogy of dimensionless spontaneous curvature  $c_0$  in Supplementary materials.

accumulation of the anisotropic components in the ICN. The driving force for the segregation of the anisotropic component originated from the mismatch between the spontaneous curvature of the anisotropic component and the membrane curvature. The inclusion of the entropy term in the minimization process reduced the segregation of the two components (Fig. 3B). Since the predicted tube connecting two cells was stable by the accumulation of the anisotropic membrane component in the tube, our attention in the following section was focused on the membrane nanotube without the parent neighboring cells.

#### 4. The curvature-dependent flux and force along the ICN

The aim of the present computational model was to determine the curvature-dependent mechanisms driving the transport of membrane components and cell organelles along the ICN. The isotropic and anisotropic curved membrane domains were considered as orientational disordered and orientational ordered membrane nanodomains, respectively. The effects of changes in the spontaneous curvature and the density of the isotropic component on the component flux along the ICN were investigated. A transient change in the density of the isotropic component could occur due to the difference in chemical potential between the two cells connected by the ICN. As before, the relative density of the isotropic component was denoted as  $\phi$ , while the density of the anisotropic component was  $1 - \phi$ . The differentiation of the membrane free energy (Eq. (1)) with respect to  $\phi$  yields the flux of the isotropic component along the ICN. Similarly, the membrane restoring force was derived from the differentiation of the membrane bending energy with respect to the membrane deformation ( $h(z)$ ).

For the sake of simplicity, the two membrane leaflets were modeled as a single contour, which was composed of isotropic (A) and anisotropic (B) components (Fig. 2). The model included only the ICN, i.e. it excluded the neighboring cells (Fig. 4). The underlying assumption was that the connected cells would have a local effect on the dynamics of the membrane component at the two endings of the ICN.

#### 4.1. The curvature-dependent flux of the isotropic component

The concentration of the isotropic component could be different between the two cells connected by the ICN. Consequently, there could be an influx of the isotropic component from the parent cell membrane into the ICN, perturbing the isotropic component density away from equilibrium. The curvature-dependent flux ( $J$ ) of the isotropic component in the plane of the membrane was obtained from the equation of motion, as follows: [22]

$$J = -\frac{\Lambda\phi(z)}{\phi_s} \nabla \cdot \frac{\partial f}{\partial \phi(z)}, \quad (3)$$

where  $z$  is the length along the horizontal axis of the tube,  $\phi_s$  is the saturation density of the isotropic component,  $\Lambda$  is the mobility of the isotropic component in the membrane ( $\Lambda = \frac{D_f}{kT}$ , where  $D_f$  is the diffusion constant),  $f$  is  $F/dA$ , and  $dA$  is the infinitesimal area of the axisymmetric model (up to quadratic order) ( $dA = r(z) \left(1 + \frac{1}{2} h'(z)^2\right) 2\pi dz$ ) [24]. Note that the negative sign on the right hand side is due to the system tendency towards equilibrium.

To shed light on the curvature-dependent flux along the ICN, we analyzed the effects of changes in the isotropic component density and intrinsic curvature on the component flux for small ( $r_t = 0.1 \mu\text{m}$ ) tube radii (Fig. 5). For  $r_t = 0.1 \mu\text{m}$ , the total flux was negative, driving the repulsion of the isotropic component along the ICN (Fig. 5A). The effects of changes in the intrinsic curvature of the isotropic component ( $H_m^A$ ) were also investigated (Fig. 5B). Similarly, it was shown that the total flux of the isotropic component was negative. To conclude, the tube was not energetically favorable to the presence of the isotropic component.

#### 4.2. The curvature-dependent force on the vesicular dilation

A vesicular dilation is repeatedly formed during the transport of a large organelle along the ICN. In this section, we analyzed whether

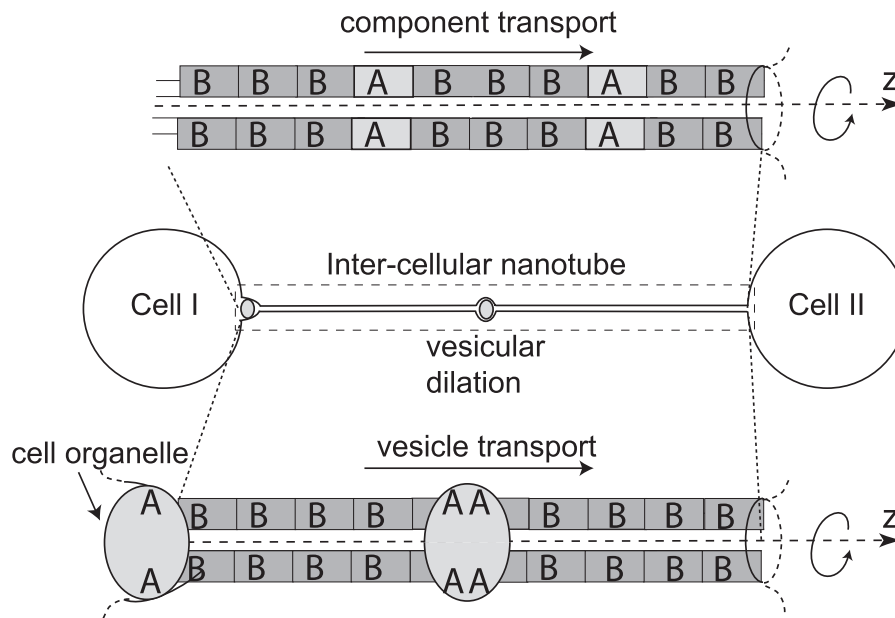


**Fig. 4.** Schematic figure of the model describing membrane component transport and organelle transport along the ICN. The highly curved tubular structure of the ICN can be stabilized by the accumulation of the anisotropic component (denoted by B) (see Fig. 2). The mismatch between the spontaneous curvature of the isotropic component (denoted by A) and the tube curvature is proposed to drive the component transport along the ICN (top panel). Due to the large size and rigidity of a cell organelle, the organelle incorporation into the tube is responsible for the formation of a vesicular dilation that favors the spontaneous curvature of the isotropic component (bottom panel). The membrane restoring force, due to membrane tension and membrane composition, could drive the vesicle transport along the ICN.

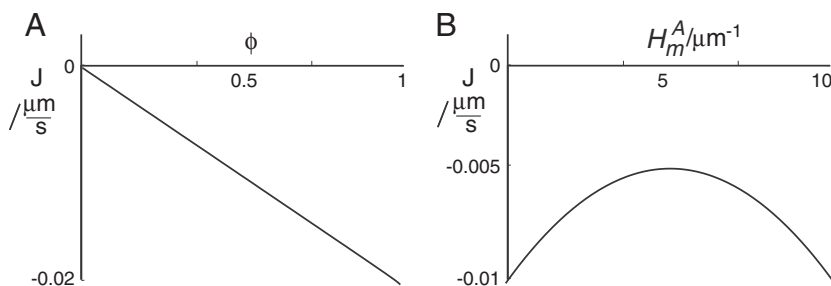


**Fig. 5.** The curvature-dependent flux of the isotropic component along the ICN. The flux ( $J$ ) of the isotropic component is plotted as a function of its relative density (A) and intrinsic (spontaneous) curvature (B). It is demonstrated that the flux is negative, predicting the efflux of the isotropic component out of the tube. The parameter values used for the analysis are as follows:  $\phi_s = 10 \mu\text{m}^{-2}$ ,  $H_m^A = 0 \mu\text{m}^{-1}$ ,  $H_m^B = 5 \mu\text{m}^{-1}$ ,  $D_m^A = 0 \mu\text{m}^{-1}$ , and  $D_m^B = 5 \mu\text{m}^{-1}$ .

the isotropic components residing at the dilation would oppose or facilitate the formation of the vesicular dilation.

The differentiation of the free energy with respect to the membrane deformation gave a vertical force exerted on the vesicular dilation. This vertical force is given by:

$$\varphi \frac{\partial h(z)}{\partial t} = - \frac{\partial f}{\partial h(z)}, \quad (4)$$

where  $\varphi$  is the friction coefficient describing the drag of the fluid surrounding the membrane, and  $t$  is time (for more details see online Supplementary material).

In Fig. 6, we plot the membrane force as a function of the dilation amplitude and of the isotropic component relative density. The membrane dilation is considered as a membrane deformation of circular shape, which is represented in polar coordinates (Fig. 6A). The curvature-dependent force was due to the difference between the spontaneous curvature of the components residing at the dilation and the dilation curvature. There was an almost linear relationship between the membrane restoring force and the dilation amplitude (Fig. 6B). When the isotropic component density was sufficiently high, the membrane force became positive, which would facilitate the formation of the vesicular dilation (Fig. 6C).

## 5. Discussion and conclusions

In the present study, we first showed experimental results revealing the preferential distribution of CTB–GM1 complexes on the spherical plasma membrane and of cholesterol–sphingomyelin rafts on the membrane leading edge and ICNs (Fig. 1). In agreement with previous studies, we propose that CTB–GM1 complexes and cholesterol–sphingomyelin rafts might have isotropic and anisotropic spontaneous curvatures, respectively. To elucidate the observed spatial distribution, we constructed a two-component model, which included an isotropic and anisotropic membrane component (Fig. 2). The system bending energy of a membrane nanotube connecting two spherical compartments attained its minimum upon the accumulation of the anisotropic component in the tube and the isotropic component in the spherical compartments (Fig. 3). The computational model was extended to consider the axisymmetric shape of an ICN, while excluding the neighboring cells (Fig. 4). The differentiation of the system free energy with respect to the density of the isotropic component ( $\phi$ ) and with respect to the membrane deformation size in the radial direction yields a curvature-dependent flux of the isotropic component and a curvature-dependent membrane force respectively. The mismatch between the intrinsic curvature of the isotropic component ( $H_m^A$ ) and the tube curvature could be responsible for the component repulsion from the ICN (Fig. 5). The effect of the isotropic spontaneous curvature on the formation of a vesicular dilation was also investigated (Fig. 6). The curvature-dependent membrane force would oppose the

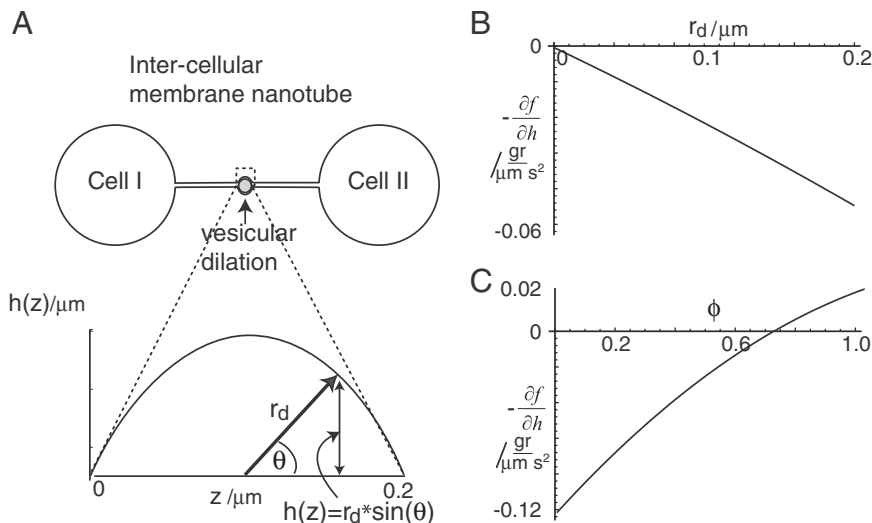


**Fig. 6.** The curvature-dependent membrane force exerted on the vesicular membrane dilation. The vesicular dilation is modeled using polar coordinates, where the dilation radius is  $r_d$ , the dilation polar coordinate is  $\theta$ , and the dilation amplitude is  $h(z)$  (A). The membrane restoring force ( $-\frac{\partial f}{\partial h}$ ) is increased linearly with the dilation amplitude (B). Note that the force is negative, being exerted to flatten the dilation back to equilibrium state. The membrane force is also plotted as a function of the relative density of the isotropic component ( $\phi$ ) (C). When the spontaneous curvature of the isotropic component is sufficiently large, the exerted force becomes positive, which could facilitate the formation of the vesicular dilation. The parameter values used for the analysis are as follows:  $H_m^A = 0 \mu\text{m}^{-1}$ ,  $H_m^B = 5 \mu\text{m}^{-1}$ ,  $D_m^A = 0 \mu\text{m}^{-1}$ ,  $D_m^B = 5 \mu\text{m}^{-1}$ ,  $\kappa = 100 \text{ kT}$ ,  $r_t = 0.1$ , and  $r_d = 0.1 \mu\text{m}$ .

formation of the vesicular dilation, when the isotropic component was a minority along the tube. On the other hand, when the spontaneous curvature of the isotropic component was greater than the curvature of the vesicular dilation, the formation of the vesicular dilation could be facilitated by the isotropic component (Fig. 6C).

In agreement with previous theoretical studies [17,37,18,34], the system bending energy was minimized upon the accumulation of the anisotropic membrane component in the tubular membrane nanotube and the isotropic membrane component in the connected cell membranes (Fig. 3). The segregation of components was due to the mismatch between the spontaneous curvature of the isotropic component and the tube curvature, while the tube curvature was more favorable by the anisotropic component [3,16,41]. In artificial systems, it was revealed that the application of pressure on one of the connected vesicles increased the rate of membrane component and cytoplasm transport along the ICN in a direction towards the tensed vesicle [19,4]. The present model hypothesis was that changes in membrane tension were due to changes in the spontaneous curvature of the membrane components residing along the ICN (Fig. 3). The advantage of the tension-mediated transport is that the component flux might not depend on chemical energy invested for the movement of molecular motors.

Previous experiments revealed that the incorporation of an organelle, possibly by molecular motors, into the ICN resulted in a vesicular dilation [12,2]. The encapsulation of the organelle could also be driven by adhesion-based mechanism at the dilation or by changes in the spontaneous curvature of the residing membrane components. A vesicular dilation might also be formed spontaneously by a rapid change in membrane composition, where the aggregation of isotropic membrane components could induce the spontaneous formation of the dilation at any location along the ICN. It is here proposed that the incorporation of the organelle would disrupt the membrane component orientational ordering at the membrane dilation, thereby leading to the formation of an orientational disordered state of different spontaneous curvature. The rapid shift from orientationally ordered to orientationally disordered state could then facilitate the incorporation of the organelle and its transport (Fig. 7). The chemical gradient between the two cells connected by the ICN could influence the direction of movement, perturbing the dilation asymmetrically. Consequently, the membrane force exerted on the dilation would have a positive projection along the ICN horizontal axis (Fig. 7). It is also possible that the pulling of the vesicle by microtubules may disrupt the vesicle shape, accounting for the asymmetrical perturbation.

The increase in membrane surface area due to membrane dilation and stretching could also disrupt the ordering and orientation of membrane components, resulting in orientationally disordered states (Fig. 7). It has been previously observed that the change in membrane surface attendant to the propagation of electrical and chemical signals was accompanied by the release of energy [13,14]. Therefore, it could be possible that the release of energy due to the change in the orientational ordering of membrane domains would facilitate the propagation of the vesicular dilation. While the isotropic component could represent also a charged lipid, the full separation of the anisotropic nanodomains might facilitate the propagation of charged lipids along the ICN.

To summarize, the present study revealed that the spatial distribution of membrane components might depend on their shape and spontaneous curvature. The transport of the membrane component and the formation of the vesicular dilation could depend on the component spontaneous curvature. Our computational model could be extended using large scale numerical simulations in order to explore the curvature-dependent dynamics of isotropic and anisotropic membrane components along highly curved structures. Experimentally, it would be possible to investigate the profile of component transport along the ICN by using a single-particle tracking (SPT) system built onto a confocal laser scan microscope. A membrane component of a planar shape introduced into the ICN could be actively

transported according to the curvature mismatch between the component spontaneous curvature and the tube curvature. To conclude, understanding the relationship between the component spontaneous curvature, the membrane geometry, and the ensuing transport, would help to understand curvature-mediated fluxes and forces not only in ICNs but also in other highly curved structures, such as membrane protrusions, membrane invaginations, and fusion pores.

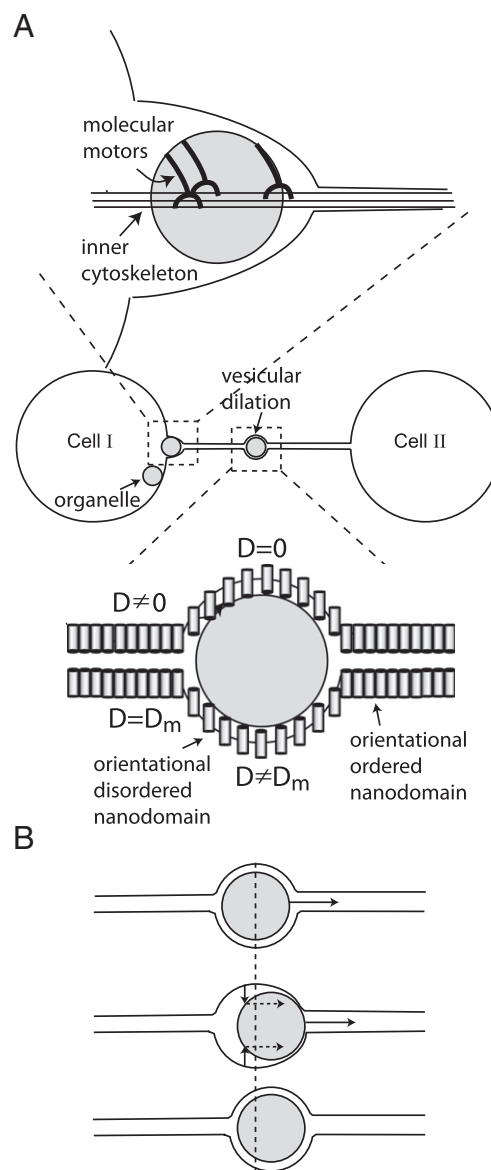


**Fig. 7.** Schematic diagram for the possible mechanisms responsible for the incorporation and transport of an organelle. The incorporation and transport of an organelle could be driven by molecular motors moving on the inner cytoskeleton (A; top inset). Additionally, the incorporation of an organelle may shift the membrane state from orientationally ordered to orientationally disordered only at the region of membrane dilation (A; bottom inset). The deviatoric membrane curvature ( $D$ ) is zero at the dilation and non-zero along the tube. Due to the difference between the deviatoric curvature of the orientationally disordered dilation ( $D_m$ ) and the actual dilation deviatoric curvature ( $D$ ), the membrane restoring force can oppose the formation of the vesicular dilation. Since the organelle is too rigid, the restoring membrane force may propel the organelle along the tube in the direction of chemical gradient or pulling by microtubules (horizontal arrow) between the two connected cells (B). The force due to the chemical gradient or due to the pulling by microtubules can perturb the dilation symmetry, leading to a net positive force projected onto the horizontal direction (dashed arrows).

## Acknowledgment

This work was supported by ARRS grants J3-2120, J1-4109, J1-4136, J3-4108 and P2-0232. The work of Nataliya Bobrovska was realized within the International PhD Projects Programme of the Foundation for Polish Science, cofinanced by the European Regional Development Fund within Innovative Economy Operational Programme Grants for innovation.

## Appendix A. Supplementary data

Supplementary data to this article can be found online at doi:10.1016/j.bioelechem.2012.02.009.

## References

- [1] S. Berne, I. Križaj, F. Pohleven, T. Turk, P. Maček, K. Sepčič, Pleurotus and Agroclybe hemolysins, new proteins hypothetically involved in fungal fruiting, *Biochim. Biophys. Acta* 1570 (2002) 153–159.
- [2] N.V. Bukoreshtliev, X. Wang, E. Hodneland, S. Gurke, J.F. Barroso, H.H. Gerdes, Selective block of tunneling nanotube (TNT) formation inhibits intercellular organelle transfer between pc12 cells, *FEBS Lett.* 583 (2009) 1481–1488.
- [3] D. Corbeil, K. Röper, C.A. Fargeas, A. Joester, W.B. Huttner, Prominin: a story of cholesterol, plasma membrane protrusions and human pathology, *Traffic* 2 (2001) 82–91.
- [4] P.G. Dommersnes, O. Orwar, F. Brochard-Wyart, J.F. Joanny, Marangoni transport in lipid nanotubes, *Europhys. Lett.* 70 (2005) 271–277.
- [5] G.P. Dubey, S. Ben-Yehuda, Intercellular nanotubes mediate bacterial communication, *Cell* 144 (2011) 590–600.
- [6] T. Fischer, Bending stiffness of lipid bilayers. III. Gaussian curvature, *J. Phys. II* 2 (1992) 337–343.
- [7] M. Fošnarič, K. Bohinc, D.R. Gauger, A. Iglič, V. Kralj-Iglič, S. May, The influence of anisotropic membrane inclusions on curvature elastic properties of lipid membranes, *J. Chem. Info. Model.* 45 (2005) 1652–1661.
- [8] U. Gimsa, V. Kralj-Iglič, A. Iglič, S. Fiedler, M. Zwanzig, L. Jonas, J. Gimsa, in: A. Leitmannova Liu (Ed.), *Basic cell–cell and cell–surface interactions in liposome and cellular systems*, Advances in Planar Lipid Bilayers and Liposomes, vol. 11, Elsevier, Amsterdam, 2007, pp. 229–251.
- [9] W.T. Gózdź, Spontaneous curvature induced shape transformations of tubular polymersomes, *Langmuir* 20 (2004) 7385–7391.
- [10] W.T. Gózdź, Influence of spontaneous curvature and microtubules on the conformations of lipid vesicles, *J. Phys. Chem. B* 109 (2005) 21145–21149.
- [11] W.T. Gózdź, The interface width of separated two-component lipid membranes, *J. Phys. Chem. B* 110 (2006) 21981–21986.
- [12] K. Gousset, E. Schiff, C. Langevin, Z. Marijanovic, A. Caputo, D.T. Browman, N.C. Fabrice de Chaumont, A. Martino, J. Enninga, J.C. Olivo-Marin, D. Männel, C. Zurzolo, Prions hijack tunnelling nanotubes for intercellular spread, *Nat. Cell Biol.* 11 (2009) 328–336.
- [13] T. Heimburg, A.D. Jackson, On soliton propagation in biomembranes and nerves, *PNAS* 102 (2005) 9790–9795.
- [14] E.V. Vargas, A. Ludu, R. Hustert, P. Gumrich, A.D. Jackson, T. Heimburg, Periodic solutions and refractory periods in the soliton theory for nerves and the locust femoral nerve, *Biophys. Chem.* 153 (2011) 159–167.
- [15] J. Hurtig, T. Chiu, B. Onfelt, Intercellular nanotubes: insights from imaging studies and beyond, *Wiley Interdiscip. Rev. Nanomed. Nanobiotechnol.* 2 (2010) 260–276.
- [16] A. Iglič, H. Hägerstrand, P. Veranič, A. Plemenitaš, B. Kralj-Iglič, Curvature induced accumulation of anisotropic membrane components 29 and raft formation in cylindrical membrane protrusions, *J. Theor. Biol.* 240 (2006) 368–373.
- [17] A. Iglič, B. Babnik, M. Fošnarič, H. Hägerstrand, V. Kralj-Iglič, On the role of anisotropy of membrane constituents in formation of a membrane neck during budding of multicomponent membrane, *J. Biomech.* 40 (2007) 579–585.
- [18] J. Jorgačevski, M. Fošnarič, N. Vardjan, M. Stenovc, M. Potokar, M. Kreft, V. Kralj-Iglič, A. Iglič, R. Zorec, Fusion pore stability of peptidergic vesicles, *Mol. Membr. Biol.* 27 (2010) 65–80.
- [19] R. Karlsson, A. Karlsson, O. Orwar, Marangoni transport in lipid nanotubes, *J. Phys. Chem. B* 107 (2003) 11201–11207.
- [20] D. Kabaso, E. Gongadze, Š. Perutková, V. Kralj-Iglič, C. Matschegewski, U. Beck, U. van Rienen, A. Iglič, Mechanics and electrostatics of the interactions between osteoblasts and titanium surface, *Comput. Methods Biomech. Biomed. Eng.* 14 (2011) 469–482.
- [21] D. Kabaso, E. Gongadze, P. Elter, K.U. van Rienen, J. Gimsa, A. Iglič, Attachment of rod-like (BAR) and membrane shape, *Mini Rev. Med. Chem.* 11 (2011) 272–282.
- [22] D. Kabaso, R. Shlomovitz, K. Schloen, T. Stradal, N.S. Gov, Theoretical model for cellular shapes driven by protrusive and adhesive forces, *PLoS Comput. Biol.* 7 (2011) 1–13.
- [23] D. Kabaso, M. Lokar, V. Kralj-Iglič, P. Veranič, A. Iglič, Temperature, cholera toxin-B and degree of malignant transformation are factors that influence formation of membrane nanotubes in urothelial cancer cell lines, *Int. J. Nanomed.* 6 (2011) 495–509.
- [24] D. Kabaso, N. Bobrovska, N.S. Gov, V. Kralj-Iglič, P. Veranič, A. Iglič, On the role of membrane anisotropy and BAR proteins in the stability of tubular membrane structures, *J. Biomech.* 45 (2012) 231–238.
- [25] G. Koster, M. VanDuijn, B. Hof, M. Dogterom, Membrane tube formation from giant vesicles by dynamic association of motor proteins, *Proc. Natl. Acad. Sci. U. S. A.* 100 (2003) 15583–15588.
- [26] V. Kralj-Iglič, V. Heinrich, S. Svetina, B. Zeks, Free energy of closed membrane with anisotropic inclusions, *Eur. Phys. J. B* 10 (1999) 5–8.
- [27] A. Iglič, H. Hägerstrand, M. Bobrowska-Hägerstrand, V. Arrigler, V. Kralj-Iglič, Possible role of phospholipid nanotubes in directed transport of membrane vesicles, *Phys. Lett. A* 310 (2003) 493–497.
- [28] M. Lokar, A. Iglič, P. Veranič, Protruding membrane nanotubes: attachment of tubular protrusions to adjacent cells by several anchoring junctions, *Protoplasma* 246 (2010) 81–87.
- [29] J. Park, S. Bauer, K. von der Mark, P. Schmuki, Nanosize and vitality: TiO<sub>2</sub> nanotube diameter directs cell fate, *Nano Lett.* 7 (2007) 1686–1691.
- [30] J. Park, S. Bauer, P. Schmuki, K. von der Mark, Narrow window in nanoscale dependent activation of endothelial cell growth and differentiation on TiO<sub>2</sub> nanotube surfaces, *Nano Lett.* 9 (2009) 3157–3164.
- [31] J. Park, S. Bauer, K.A. Schlegel, F.W. Neukam, K.V. Mark, P. Schmuki, TiO<sub>2</sub> nanotube surfaces: 15 nm—optimal length scale of surface topography for cell adhesion and differentiation, *Small* 5 (2009) 666–671.
- [32] B.J. Peter, H.M. Kent, I.G. Mills, Y. Vallis, P.J. Butler, P.R. Evans, H.T. McMahon, BAR domains as sensors of membrane curvature: the amphiphysin BAR structure, *Science* 303 (2004) 495–499.
- [33] A. Rustom, R. Saffrich, I. Markovic, P. Walther, H. Gerdes, Nanotubular highways for intercellular organelle transport, *Science* 303 (2004) 1007–1010.
- [34] H.J. Risselada, S.J. Marrink, M. Müller, Curvature-dependent elastic properties of liquid-ordered domains result in inverted domain sorting on uniaxially compressed vesicles, *Phys. Rev. Lett.* 106 (2011) 148102.
- [35] S. Sonnino, L. Mauri, V. Chigorno, A. Prinetti, Gangliosides as components of lipid membrane domains, *Glycobiology* 17 (2006) 1–13.
- [36] B. Sorre, A. Callan-Jones, J.B. Manneville, P. Nassoy, J.F. Joanny, J. Prost, B. Goud, P. Bassereau, Curvature-driven lipid sorting needs proximity to a demixing point and is aided by proteins, *Proc. Natl. Acad. Sci. U. S. A.* 106 (2009) 5622–5626.
- [37] A. Tian, T. Baumgart, Sorting of lipids and proteins in membrane curvature gradients, *Biophys. J.* 96 (2009) 2676–2688.
- [38] C. Vidulescu, S. Clejan, K. O'Connor, Vesicle traffic through intercellular bridges in du 145 human prostate cancer cells, *J. Cell. Mol. Med.* 8 (2004) 88–96.
- [39] P. Veranič, M. Lokar, G.J. Schuetz, J. Weghuber, S. Wieser, H. Hägerstrand, V. Kralj-Iglič, A. Iglič, Different types of cell-to-cell connections mediated by nanotubular structures, *Biophys. J.* 95 (2008) 4416–4425.
- [40] S.C. Watkins, R.D. Salter, Functional connectivity between immune cells mediated by tunneling nanotubes, *Immunity* 23 (2005) 309–318.
- [41] A. Weigmann, D. Corbeil, A. Hellwig, W.B. Huttner, Prominin, a novel microvilli-specific polytopic membrane protein of the apical surface of epithelial cells, is targeted to plasmalemmal protrusions of non-epithelial cells, *Proc. Natl. Acad. Sci. U. S. A.* 74 (1997) 12425–12430.